Inorganic Chemistry
Article

Inorg. Chem. **2010**, *49*, 7401–7413 **7401**
DOI: 10.1021/ic100583f

Structural, Transport, and Electrochemical Investigation of Novel $AMSO_4F$ (A = Na, Li; M = Fe, Co, Ni, Mn) Metal Fluorosulphates Prepared Using Low Temperature Synthesis Routes

Prabeer Barpanda,[†] Jean-Noël Chotard,[†] Nadir Recham,[†] Charles Delacourt,[†] Mohamed Ati,[†] Loic Dupont,[†] Michel Armand,[†] and Jean-Marie Tarascon*[,†,‡]

[†]*Laboratoire de Réactivité et Chimie des Solides, Université de Picardie Jules Verne, CNRS UMR 6007, 33 rue Saint Leu, 80039, Amiens, France, and* [‡]*Materials Department, University of California Santa Barbara, California 93106*

Received March 29, 2010

We have recently reported a promising 3.6 V metal fluorosulphate ($LiFeSO_4F$) electrode, capable of high capacity, rate capability, and cycling stability. In the current work, we extend the fluorosulphate chemistry from lithium to sodium-based systems. In this venture, we have reported the synthesis and crystal structure of $NaMSO_4F$ candidates for the first time. As opposed to the triclinic-based $LiMSO_4F$ phases, the $NaMSO_4F$ phases adopt a monoclinic structure. We further report the degree and possibility of forming $Na(Fe_{1-x}M_x)SO_4F$ and $(Na_{1-x}Li_x)MSO_4F$ (M = Fe, Co, Ni) solid-solution phases for the first time. Relying on the underlying topochemical reaction, we have successfully synthesized the $NaMSO_4F$, $Na(Fe_{1-x}M_x)SO_4F$, and $(Na_{1-x}Li_x)MSO_4F$ products at a low temperature of 300 °C using both ionothermal and solid-state syntheses. The crystal structure, thermal stability, ionic conductivity, and reactivity of these new phases toward Li and Na have been investigated. Among them, $NaFeSO_4F$ is the only one to present some redox activity (Fe^{2+}/Fe^{3+}) toward Li at 3.6 V. Additionally, this phase shows a pressed-pellet ionic conductivity of 10^{-7} $S \cdot cm^{-1}$. These findings further illustrate the richness of the fluorosulphate crystal chemistry, which has just been recently unveiled.

Introduction

Since Sony met success in commercializing its rechargeable Li-ion batteries, these systems have seen manifold developments in the last two decades to become an integral part of portable electronics, telecommunication and computing devices, and are currently on the anvil to enter into the EV/HEV market. For successful and secure applications, electrodes should have high operating voltage, energy density, and rate capability along with low cost and an environmentally benign nature.[1−3] In the quest for better batteries, various electrodes have been developed with different structures such as layered structure ($LiCoO_2$, $LiCo_{1/3}Ni_{1/3}Mn_{1/3}O_2$),[4,5] spinel structure ($LiMn_2O_4$, $LiMn_{3/2}Ni_{1/2}O_4$),[6,7] olivine structure ($LiFePO_4$),[8] tavorite structure ($LiFePO_4F$, $LiFePO_4OH$)[9] and so forth. At present, for safety, olivine-$LiFePO_4$ with a redox voltage of 3.42 V and a theoretical capacity of 171 mA $h \cdot g^{-1}$ is most widely pursued in both academic and industrial arenas. Benchmarking against $LiFePO_4$, the research world pursues the identification of novel electrodes combining good cost, conductivity, capacity, and the same expected safety due to a scaffold structure. In such an effort, we have recently reported $LiFeSO_4F$, a 3.6 V electrode delivering a high capacity of 140 mA $h \cdot g^{-1}$ with good rate capability and cycling stability[10] without any need for carbon coatings or particles downsizing. Here, the high open circuit potential is a combined result of sulfate $(SO_4)^{2-}$ substitution of polyanionic phosphates $(PO_4)^{3-}$ and fluorine (F^-) induced larger ionicity.[11] These tavorite-structure based metal fluorosulphates have interconnected MO_4F_2 octahedra and SO_4 tetrahedra with tunnels along [100], [010], [101], and [111] directions facilitating ion insertion/de-insertion.[10]

*To whom correspondence should be addressed. E-mail: jean-marie.tarascon@sc.u-picardie.fr.

(1) Tarascon, J.-M.; Armand, M. *Nature* **2001**, *414*, 359–367.
(2) Winter, M.; Besenhard, J. O.; Spahr, M. E.; Novàk, P. *Adv. Mater.* **1998**, *10*, 725–763.
(3) Armand, M.; Tarascon, J.-M. *Nature* **2008**, *451*, 652–657.
(4) Mizushima, K.; Jones, P. C.; Wiseman, P. C.; Goodenough, J. B. *Mater. Res. Bull.* **1980**, *15*(6), 783–789.
(5) Yabuuchi, N.; Makimura, Y.; Ohzuku, T. *J. Electrochem. Soc.* **2007**, *154*(4), A314–A321.
(6) Tarascon, J.-M.; Guyomard, D. *Solid State Ionics* **1994**, *69*, 222–237.
(7) Zhong, Q.; Bonakdarpour, A.; Zhang, M.; Gao, Y.; Dahn, J. R. *J. Electrochem. Soc.* **1997**, *144*(1), 205–213.
(8) Padhi, A. K.; Nanjundaswamy, K. S.; Goodenough, J. B. *J. Electrochem. Soc.* **1997**, *144*(4), 1188–1194.
(9) Barker, J.; Saidi, M. Y.; Swoyer, J. L. International Patent WO0184655.
(10) Recham, N.; Chotard, J.-N.; Dupont, L.; Delacourt, C.; Walker, W.; Armand, M.; Tarascon, J.-M. *Nat. Mater.* **2010**, *9*(1), 68–75.
(11) Padhi, A. K.; Manivannan, V.; Goodenough, J. B. *J. Electrochem. Soc.* **1998**, *145*(5), 1518–1520.

Published on Web 07/14/2010

On another note, cost and resource availability do impact the battery community, which has led to the growing use of Mn-, Ti-, and Fe-based electrodes instead of Co- or Ni-based ones. Along the same line, increasing fears regarding Li availability and prices are driving new chemistries. Within this context, Na-based compounds are being considered for the next generation energy-storage devices, resulting in the renewed interest for reversible Na-based electrodes such as Na_2FePO_4F and $NaVPO_4F$.[12−15] Although at a nascent stage, Na-based intercalation compounds are promising with their capacity for fast Na−Li ion exchange and successful use of hard carbons as anodes reaching a capacity as high as 300 mA h·g^{-1}.[16,17] Encouraged by this, we pursued to extend the Li-based metal fluorosulphate systems ($LiMSO_4F$) to their Na-counterparts ($NaMSO_4F$).

This opens up a variety of questions. Do the $NaMSO_4F$ phases adopt the same crystal structure like $LiMSO_4F$? Is it feasible to exchange Na with Li and study the underlying ion-exchange mechanism? What is the feasibility of substituting the M site for various transition metal elements? Can we form a solid solution between $NaMSO_4F$−$LiMSO_4F$ phases? In an effort to answer these queries, we attempted to synthesize $NaMSO_4F$ (M = Fe, Co, Ni, Mn) end members as well as $Na(Fe_{1-x}M_x)SO_4F$ (M = Co, Ni, Mn) and $(Na_{1-x}Li_x)MSO_4F$ (M = Fe, Co, Ni, Mn) mixed phases by adopting both a low-temperature (300 °C) ionothermal synthesis route and a solid-state (ceramic) synthesis. We have described both syntheses of various metal fluorosulphate materials. The structure of various isostructural $NaMSO_4F$ phases has been reported for the first time. The effect of crystal structure on the ionic conductivity, ion-exchange reaction, and overall electrochemical performance has been described to gauge the potential of these novel sodium-based metal fluorosulphate phases for energy-storage applications.

Experimental Section

Synthesis of $AMSO_4F$ Fluorosulphates (A = Na, Li; M = Co, Ni, Mn). Thanks to the use of ionothermal synthesis, practically unknown to inorganic chemists, we have succeeded in preparing $LiFeSO_4F$,[10] which turns out to decompose at 360 °C as well as in water, explaining why this metastable phase was never made before. Ionic liquids are presently costly. Although they can be recovered, large-volume production suggests to look for synthesis alternatives. Ceramic approaches under autogenous pressure were tried to stabilize fluorosulphates. This was feasible with a few but not all of them, $LiFeSO_4F$ being the less cooperative. Consequently, the materials reported herein were prepared by either a ceramic or an ionothermal approach under the conditions described below.

Solid-State Synthesis. For solid-state (ceramic) synthesis of sodium-based metal fluorosulphates, corresponding metal sulfate monohydrates ($MSO_4·H_2O$, M = Fe, Co, Ni, Mn) and NaF were taken as precursors. Here, monohydrate precursors are specifically used as the product formation occurs via topochemical reaction.[10,18] These monohydrate precursors can be easily prepared from commercially available $MSO_4·7H_2O$ powders as described in a previous report.[18] Stoichiometric amounts of these precursors [with slight excess (≈ 5 mol%) of NaF] were mixed for 5 min in a Spex-5000 shock-type miller to form 1 g of final product. The precursor mixture was pressed into pellets by uniaxial press (10 MPa). These pellets were loaded inside Teflon-lined Parr reactors sealed under Ar atmosphere and were annealed at 300 °C for 40−50 h with an autogenous pressure of 3 bar. The recovered pellets were ground, washed with ethyl acetate/dichloromethane, and oven-dried for further analysis. $NaMnSO_4F$ only can be synthesized by annealing a stoichiometric mixture of NaF and anhydrous $MnSO_4$ at 500 °C for 2 h in air or 550 °C for 12 h in Ar atmosphere. The 3d-metal substituted $Na(Fe_{1-x}M_x)SO_4F$ (M = Co, Ni, Mn) phases were prepared by following the same method and using an equimolar mixture [with slight excess (≈5 mol%)] of NaF and $(Fe_{1-x}M_x)SO_4·H_2O$ precursors. The preparation of $(Fe_{1-x}M_x)SO_4·H_2O$ monohydrate precursors is described elsewhere.[18] Further, mixed cations-based $(Na_{1-x}Li_x)MSO_4F$ phases were prepared following a similar method using stoichiometric mixtures of NaF, LiF, and $MSO_4·H_2O$ precursors.

Ionothermal Synthesis. When specified within the text, using mixtures of the same precursors as that of the ceramic route, the ionothermal synthesis was conducted using EMI-TFSI [1-Ethyl-3-methylimidazolium bis(TriFluoromethanesulfonyl Imide)] ionic liquid media. Stoichiometric amounts of precursor mixture were taken in Teflon-lined autoclaves, 5 cm^3 of EMI-TFSI was added and stirred for 20 min to ensure proper mixing of precursors inside the ionic liquid. The autoclaves were left undisturbed for 15 min, placed inside an oven and heat-treated at 300 °C for 9 h (heating rate 5 °C.min^{-1}). Upon cooling to room temperature, the product was recuperated from ionic liquid by centrifugation, washed with dichloromethane (CH_2Cl_2) and oven-dried at 60 °C. The ionic liquid can be recuperated for further usage as described in an earlier report.[19]

Chemical Oxidation and Ion Exchange Reaction. Ion-exchange of Na^+ for Li^+ in the Na-based fluorosulphates was conducted, for times ranging from hours to days, by refluxing NO_2BF_4-based acetonitrile/cyclopentadione solutions containing fluorosulphate powders or dissolved LiCl/LiBr as a source of Li.

XRD and Rietveld Refinement. Powder X-ray diffraction (XRD) patterns of as-synthesized materials were obtained either by a Bruker D8-Advantage powder diffractometer using Cu−Kα radiation (λ_1 = 1.5405 Å, λ_2 = 1.5443 Å) equipped with a LynxEye detector or by a Bruker D8-Advantage Diffractometer with Co−Kα radiation (λ_1 = 1.7892 Å, λ_2 = 1.7932 Å) equipped with a Vantec-1 detector both operating at 40 kV and 40 mA. The diffraction patterns were collected in the 2θ range of 10−60° at a scan speed of 1°/min. The powder patterns were indexed using DICVOL, and cell parameters were refined by the full pattern matching method using the FullProf program.[20,21] Following, the temperature-controlled XRD was performed in a Bruker D8 diffractometer (Cu−Kα radiation, operating at 40 kV and 30 mA) with an attached HTK 1200 °C Anton Paar chamber. Powder diffraction patterns were recorded in the 2θ range of 14−32° for temperatures varying from room temperature (RT) to 450 °C, with a scan duration of 20 min at every intermediate temperature.

Thermal Gravimetric Analysis. Around 10 mg of powder sample, kept inside an alumina crucible, was heated from RT

(12) Ellis, B. L.; Makahnouk, W. R. M.; Makimura, Y.; Toghill, K.; Nazar, L. F. *Nat. Mater.* **2007**, *6*, 749–753.
(13) Ellis, B. L.; Makahnouk, W. R. M.; Rowan-Weetaluktuk, W. N.; Ryan, D. H.; Nazar, L. F. *Chem. Mater.* **2010**, *22*(3), 1059–1070.
(14) Recham, N.; Chotard, J.-N.; Dupont, L.; Djellab, K.; Armand, M.; Tarascon, J.-M. *J. Electrochem. Soc.* **2009**, *156*, A993–A999.
(15) Barker, J.; Saidi, M. Y.; Swoyer, J. L. *Electrochem. Solid-State Lett.* **2003**, *6*(1), A1–A4.
(16) Stevens, D. A.; Dahn, J. R. *J. Electrochem. Soc.* **2000**, *147*(4), 1271–1273.
(17) Komaba, S.; Murata, W.; Ozeki, T. *Abstracts of Papers*, 216th Meeting of the Electrochemical Society, Vienna, Austria, Oct 4−9, 2009.
(18) Barpanda, P.; Recham, N.; Chotard, J.-N.; Djellab, K.; Walker, W.; Armand, M.; Tarascon, J.-M. *J. Mater. Chem.* **2010**, *20*(9), 1659–1668.
(19) Recham, N.; Dupont, L.; Courty, M.; Djellab, K.; Larcher, D.; Armand, M.; Tarascon, J.-M. *Chem. Mater.* **2009**, *21*(6), 1096–1107.
(20) Rodríguez-Carvajal, J. Recent Developments of the Program FULLPROF. *CPD Newslett.* **2001**, *26*, 12; available at http/::www.iucr.org/iucr-top/news/index.html. The program/ documentation can be obtained from http://www.ill.fr/dif/Soft/fp.
(21) Rodríguez-Carvajal, J. *Physica B* **1993**, *192*, 55–69.

to 600 °C (heating rate = 10 °C/min) in air (50 mL.min^{-1}) regulated atmosphere, and the TGA data were collected with a Simultaneous Thermal Analyzer STA 449C Jupiter unit (Netzsch Inc.). The isothermal drift and sensitivity values are 0.6 μg h^{-1} and 0.1 μg, respectively.

Electron Microscopy. The morphology of all samples was examined with a FEI Quanta 200 F field-emission scanning electron microscope (FESEM) equipped with an energy-dispersive X-ray (EDX) spectrometer. The SEM unit was operated at 20 kV under low vacuum to avoid any charging effect. Elemental analysis and mapping was performed at several different spots to assess homogeneous distribution of constituting elements. A transmission electron microscopy (TEM) study was conducted on the powder sample deposited on a TEM holey (with carbon−copper grid) using an FEI-Tecnai F20 S-Twin electron microscope operating at 200 kV and fitted with an EDAX EDS system.

Electrical Conductivity Measurement. For conductivity measurement, dense pellets were made by pressing the metal fluorosulphate powder samples first by uniaxial press (500 kg cm^{-2}) followed by isostatic press (2500 bar). As fluorosulphates are prone to decomposition at high temperatures, the densification process was devoid of any sintering step. The ionically-blocking electrodes were gold sputtered on both faces of the pellets. Alternating current (AC) and direct current (DC) conductivity was measured by employing (AC) impedance spectroscopy (200 kHz to 10 mHz) and 1 V DC polarization (which is below the decomposition potential). These measurements were conducted at different temperatures (from RT to 140 °C) using Bio-Logic VMP3 as detailed elsewhere.[22] The activation energies (E_a) for AC and DC conductivities were calculated as per the Arrhenius relation: $\log(\delta T) = \log(\delta_0 T_0) - E_a/k_B(1/T - 1/T_0)$ (where δ = conductivity (S·cm^{-1}) and k_B = Boltzmann constant).

Electrochemical Testing. The metal fluorosulphate samples were mechanically milled with Super P carbon black in 80:20 weight ratio for 10 min (under Ar atmosphere) using a Spex-800 shock-milling machine. The electrochemical performance of these active materials was tested in standard Swagelok-type cells, using pasted sodium as anode and two sheets of Whatman GF/D borosilicate glass fiber disks as separator soaked with either 1 M $NaClO_4$ or Na-TFSI solution in propylene carbonate (PC). The cells were assembled inside an argon-filled glovebox with a typical cathode loading of 9−10 mg·cm^{-2}. Galvanostatic charge−discharge tests were performed using a MacPile (Claix, France) controller at 20 °C. Typically, the cells were cycled between 2.5 to 4.2 V versus Na^+/Na^0 at a rate of C/20 (1 Na^+ exchanged per 20 h). Cells containing Co- and Ni-based cathodes were charged up to 5 V using an aluminum current collector to avoid any stainless steel corrosion at high potential.

Results and Discussion

Synthesis of $NaMSO_4F$ End Members. Our ionothermal synthesis approach of lithium metal fluorosulphate compounds ($LiMSO_4F$; M = Fe, Co, Ni, Mn),[10,16] together with its recently developed low temperature solid-state (ceramic) one,[23] was implemented to synthesize the corresponding sodium metal fluorosulphates, with a special focus on the solid-state route for its feasibility and economy. Overall, the synthesis of $NaMSO_4F$ compounds involves two parallel steps; first the removal of the structural H_2O from the monohydrate precursor followed by the introduction of Na^+ and F^- (from NaF) ions into the structure, the overall reaction being

$$MSO_4 \cdot H_2O(s) + NaF(s) \rightleftharpoons NaMSO_4F(s) + H_2O(g)$$

As the sulfate compounds are prone to decomposition at high temperature, we conducted the synthesis at a moderate temperature of 300 °C for 40 h to ensure complete reaction (as Na^+ diffuses slowly because of its larger size).

These materials were single-phased as determined by XRD and TEM studies. The XRD patterns of the $NaMSO_4F$ end members (M = Fe, Co, Mn) are presented in Figure 1 panels a, b, and c, respectively (the case M = Ni is shown in the Supporting Information). $NaMSO_4F$ samples containing Fe, Co, and Ni were successfully indexed in a monoclinic cell with a space group $P2_1/c$. Further, using the Rietveld refinement method, the atomic coordinates were determined for $NaFeSO_4F$ and $NaCoSO_4F$ phases as given in Table 1 and 2, respectively. Selected interatomic distances of these compounds are reported in Table 3. For each $NaMSO_4F$ phase (M = Fe, Co, Ni), 38 parameters were refined in the following order: 1 for the scale, 1 for the sample shift, 4 for the cell parameters, 3 for the profile of peaks, 24 for the atomic positions, and finally 5 for the isotropic Debye−Waller factors. Although we are aware of our accuracy limitation, it is worth noting that the Fe atoms are displaced from the geometrical centers of the octahedra resulting in alternating long (2.00 Å) and short (1.88 Å) Fe−F bonds (e.g., a 0.06 Å displacement from the average octahedral center in the $+c$ direction, which occurs as well for the Co atomic positions in $NaCoSO_4F$) (Figure 2a). A similar displacement for the Fe or Co cations, but in the opposite direction, occurs within the second chain within the unit cell, which is related to the first one by a symmetric center. Similar to our earlier encounter with Mn-based phases ($LiMnSO_4F$), we found that $NaMnSO_4F$ have completely different XRD patterns than other end-members (Figure 1c), which can be fully indexed to a monoclinic structure possessing $I2/c$ space groups with lattice parameters a = 12.1635(5) Å, b = 6.6364(2) Å, c = 10.3488(4) Å, β = 105.068(2)°, and V = 806.65(5) Å^3 (with Z = 8). Interestingly, this $NaMnSO_4F$ compound has lattice parameters very close to those of Triplite $(Mn,Fe,Mg,Ca)_2(PO_4)(F,OH)$ with lattice parameters a = 12.085(1) Å, b = 6.536(1) Å, c = 9.91(1) Å, β = 105.633°, V = 753.81 Å^3 (Z = 8) or of Magniotriplite $(Mg_{0.89}Fe_{0.88}Mn_{0.23})(PO_4)F$ with lattice parameters a = 12.035(5) Å, b = 6.432(4) Å, c = 9.799(2) Å, β = 108.12(2)°, V = 720.91 Å^3 (Z = 8) so that one could think our compounds as $(Mn,Li)_2(SO_4)F$ or $(Mn,Na)_2(SO_4)F$ analogues.[24] This will imply inter site mixing that could explain both (i) the space group change from $P2_1/c$ to $I2/c$ in going from $NaFeSO_4F$ to $NaMnSO_4F$ and (ii) the inability of the $LiMnSO_4F$ to reversibly insert Li ions as previously encountered because of poorly mobile 3d cations blocking the Li-ion diffusion path. However, these structural comments, based solely on comparisons, are highly speculative and should be treated as such for the time being. We are currently in the process of solving the exact structure of Mn-based fluorosulphates (i.e., $NaMnSO_4F$ and $LiMnSO_4F$) and of understanding their structure−property relationships.[25]

(22) Delacourt, C.; Laffont, L.; Bouchet, R.; Wurm, C.; Leriche, J.-B.; Morcrette, M.; Tarascon, J.-M.; Masquelier, C. *J. Electrochem. Soc.* **2005**, *152*(5), A913–921.

(23) Ati, M.; Barpanda, P.; Recham, N.; Moulay, M.; Jumas, J. C.; Armand, M.; Tarascon, J.-M. *J. Electrochem. Soc.*, manuscript in preparation.

(24) http://webmineral.com/data/.

(25) Barpanda, P.; Chotard, J.-N.; Dupont, L.; Delacourt, C.; Armand, M.; Tarascon, J.-M. *Inorg. Chem.*, manuscript in preparation.

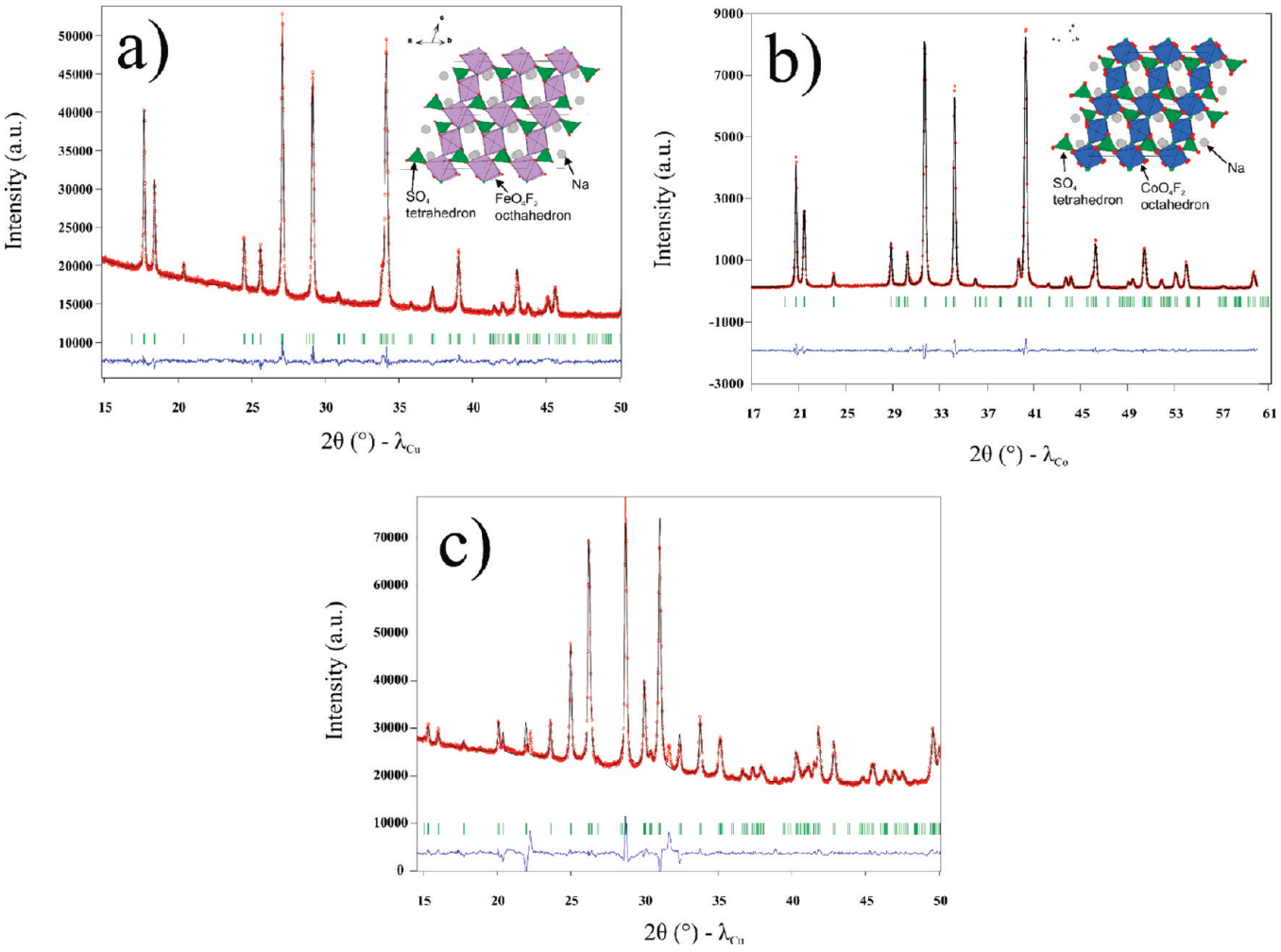

Figure 1. Powder XRD patterns for (a) $NaFeSO_4F$, (b) $NaCoSO_4F$, and (c) $NaMnSO_4F$ prepared by solid state synthesis using an equimolar mixture of corresponding metal sulfate monohydrate precursors and NaF. A typical synthesis was carried out at 300 °C for 40 h. For each case, the experimental diffraction pattern (red dots), calculated patterns (black lines), Bragg positions (green ticks), and the difference curve (blue line) are shown. The inset figures depict the respective crystal structure. While $NaFeSO_4F$ and $NaCoSO_4F$ have monoclinic structure with $P2_1/c$ symmetry, $NaMnSO_4F$ has monoclinic $I2/c$ symmetry. For $NaMnSO_4F$, the unindexed peak around 32° is due to a slight amount of Na_2SO_4 or $Na_2Mn(SO_4)_2$ impurity.

Table 1. Lattice Parameters, Cell Volume, and Atomic Coordinates for $NaFeSO_4F$ with Monoclinic ($P2_1/c$) Symmetry

$NaFeSO_4F$	a (Å)	b (Å)	c (Å)	volume (Å^3)
	6.6799(2)	8.7060(2)	7.1914(2)	383.48(2)
	$\alpha = 90°$	$\beta = 113.516(2)°$	$\gamma = 90°$	
	$\chi^2 = 2.79$	$R_p = 18.3$	$R_{wp} = 8.91$	$R_{Bragg} = 5.28$

atom	Wyckoff position	x	y	z	B_{iso}	occupancy
Na	4*e*	0.226(3)	0.9164(6)	0.253(3)	1.35(19)	1
Fe	4*e*	0.7479(19)	0.7572(10)	−0.001(2)	2.50(8)	1
S	4*e*	0.259(3)	0.9273(7)	0.762(3)	1.88(16)	1
F	4*e*	0.249(3)	0.1688(8)	0.261(4)	0.74(18)	1
O1	4*e*	0.561(2)	0.178(3)	0.087(3)	0.94(10)	1
O2	4*e*	0.360(3)	0.488(3)	0.152(3)	0.94(10)	1
O3	4*e*	0.887(2)	0.341(3)	0.890(4)	0.94(10)	1
O4	4*e*	0.151(3)	0.041(3)	0.859(3)	0.94(10)	1

Except for the Mn-homologue, all other phases have similar structures as shown in Figure 1 (insets), which belong to the titanite class of compounds (e.g., $CaTiOSiO_4$, $NaTaOGeO_4$, $NaVOPO_4$) originally reported by Zachariasen.[26−28] Similar to the $LiMSO_4F$ (triclinic), $NaMSO_4F$ (monoclinic) have chains of MO_4F_2 octahedra units (along *c*-axis) connected to each other by F vertices in a *trans* position. These MO_4F_2 chains are connected to each other by O vertices of SO_4 tetrahedra units, thus forming a 3-dimensional framework. However, the structure of $NaMSO_4F$ differs from that of $LiMSO_4F$ in terms of orientation and distortion of MO_4F_2 octahedra,

(26) Zachariasen, W. H. *Z. Kristallogr.* **1930**, *73*, 7–16.
(27) Malcherek, T. *Acta Crystallogr.* **2007**, *B63*, 545–550.
(28) Lii, K.-H.; Li, C.-H.; Chen, T.-M.; Wang, S.-L. *Z. Kristallogr.* **1991**, *197*, 67–73.

Table 2. Lattice Parameters, Cell Volume, and Atomic Coordinates for $NaCoSO_4F$ with Monoclinic ($P2_1/c$) Symmetry

$NaCoSO_4F$	a (Å)	b (Å)	c (Å)	volume (Å^3)
	6.6664(3)	8.6174(4)	7.1436(3)	373.89(3)
	$\alpha = 90°$	$\beta = 114.343(3)°$	$\gamma = 90°$	
	$\chi^2 = 2.20$	$R_p = 5.5$	$R_{wp} = 7.4$	$R_{Bragg} = 1.68$

atom	Wyckoff position	x	y	z	B_{iso}	occupancy
Na	4*e*	0.260(3)	0.9132(6)	0.239(4)	3.7(3)	1
Co	4*e*	0.7468(16)	0.7500(13)	−0.006(3)	3.00(16)	1
S	4*e*	0.257(3)	0.9319(8)	0.761(3)	2.3(3)	1
F	4*e*	0.244(4)	0.1681(14)	0.262(8)	2.6(3)	1
O1	4*e*	0.585(3)	0.177(4)	0.099(5)	1.00(19)	1
O2	4*e*	0.335(3)	0.489(3)	0.132(4)	1.00(19)	1
O3	4*e*	0.916(4)	0.340(4)	0.890(5)	1.00(19)	1
O4	4*e*	0.126(3)	0.046(3)	0.846(3)	1.00(19)	1

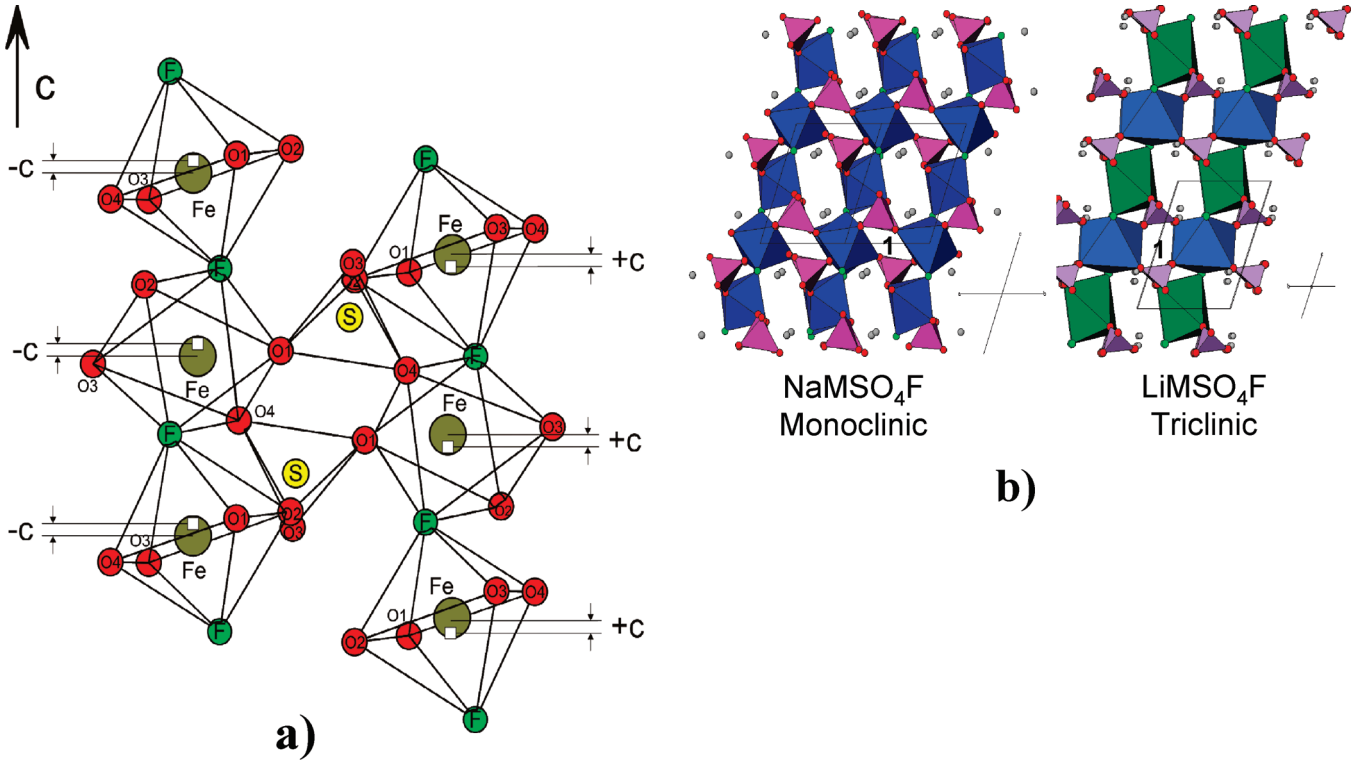

Figure 2. (a) Chains of interconnected MO_4F_2 (M = Fe) octahedra and SO_4 tetrahedra depicting the displacement of Fe atoms from their geometric centers, as shown by the white square marks. (b) The comparative crystal structures of monoclinic sodium-based and triclinic lithium based metal fluorosulphates.

as shown in Figure 2b. The shape of cavity (marked by 1) is more distorted in $NaMSO_4F$ structure. Therefore, the major difference occurs in the sodium site. While the (smaller) Li can occupy 2 sites with equal probability,[10,29] there is a fixed site for the (larger) Na atom. We intend to conduct neutron diffraction studies in the near future to obtain further structural insights on these newly-found materials. For all these phases (with four formula unit per unit cell), we could calculate the theoretical density to be 3.36, 3.49, and 3.51 g·cm^{-3} for $NaFeSO_4F$, $NaCoSO_4F$, and $NaNiSO_4F$, respectively. Figure 3(a−d) illustrates the morphology of solid-state synthesized $NaMSO_4F$ phases with micrometric particles. For $NaFeSO_4F$, the TEM study reveals particle sizes ranging from 0.5−1 μm (Figure 3e), and the corresponding SAED pattern shows an array of pseudo-hexagonal symmetry dots, which is indexed using [6−25]* zone axis (Figure 3f). Following the current work, we have recently succeeded in the low-temperature preparation of the monoclinic-structured $NaCuSO_4F$, $NaZnSO_4F$, and $NaMgSO_4F$ phases to be reported in a future communication

Table 3. Selected Interatomic Distances (Å) in $NaFeSO_4F$ and $NaCoSO_4F$ Focusing on the MO_4F_2 Octahedra and SO_4 Tetrahedra

distance (Å)	$NaFeSO_4F$	$NaCoSO_4F$
M − O1	1.99(2)	2.12(2)
M − O2	2.37(2)	2.23(3)
M − O3	2.40(2)	2.19(3)
M − O4	2.01(3)	2.08(3)
M − F	1.88(3)	1.86(6)
M − F	2.00(3)	1.98(6)
S − O1	1.56(2)	1.45(3)
S − O2	1.43(3)	1.41(4)
S − O3	1.36(3)	1.45(3)
S − O4	1.55(3)	1.59(3)

(29) Sebastian, L.; Gopalakrishnan, J.; Piffard, Y. *J. Mater. Chem.* **2002**, *12*, 374–377.

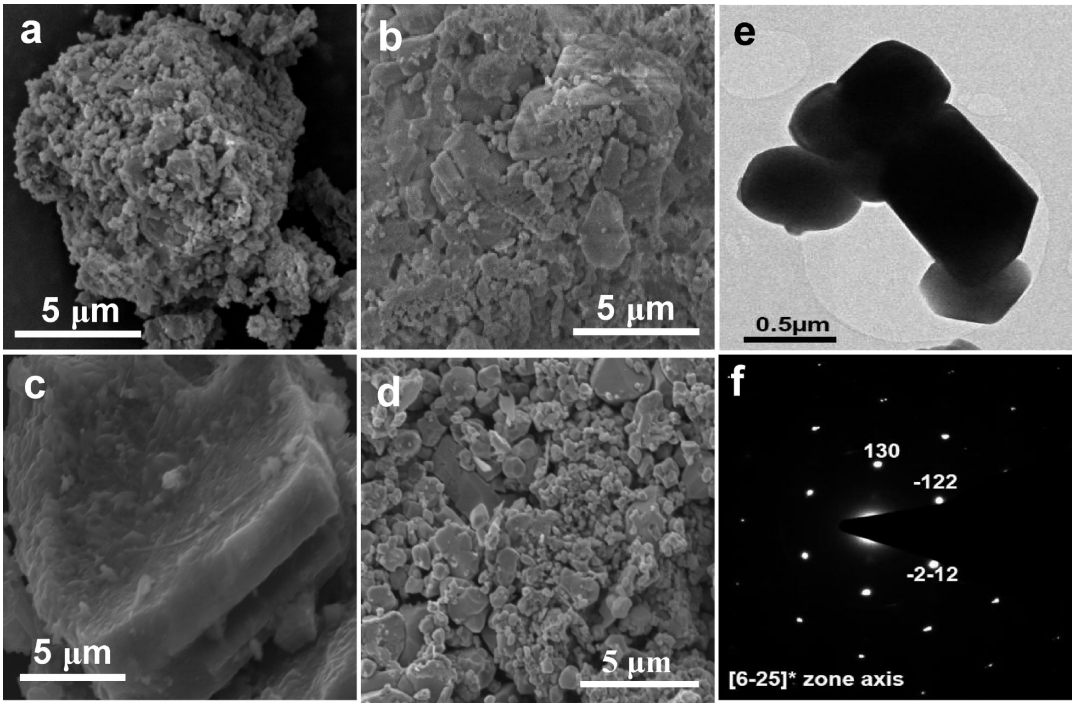

Figure 3. SEM images of solid-state synthesized (a) $NaCoSO_4F$, (b) $NaFeSO_4F$, (c) $NaNiSO_4F$, and (d) $NaMnSO_4F$. For the $NaFeSO_4F$ homologue, a TEM image (e) and corresponding SAED pattern (f) are shown.

addressing their synthesis, structure, and conductivity data.[30]

Synthesis of $Na(Fe_{1-x}M_x)SO_4F$ Solid-Solution Phases. As the synthesis of metal fluorosulphate compounds involves a topotactic reaction mechanism having a striking structural similarity between the mother precursor monohydrate phase (monoclinic with $C2/c$ symmetry) and the product phase (monoclinic with $P2_1/c$ symmetry), we have used $(Fe_{1-x}M_x)SO_4 \cdot H_2O$ precursors (where, M = Co, Ni, Mn) to fabricate 3d-transition metal-substituted $NaFeSO_4F$ compounds. These solid-solution precursors containing Fe−Co, Fe−Ni, and Fe−Mn mixing at the molecular level were synthesized by dissolution and precipitation methods as described earlier.[18] The powder XRD patterns and corresponding lattice parameters of these $(Fe_{1-x}M_x)SO_4 \cdot H_2O$ precursors are given in the Supporting Information. These precursors were reacted with NaF to obtain the corresponding $Na(Fe_{1-x}M_x)SO_4F$ phases using the same experimental protocol as for $NaMSO_4F$ end members.

The XRD patterns of Co, Ni, and Mn-substituted $Na(Fe_{1-x}M_x)SO_4F$ members were collected and are reported in Figure 4 for the $Na(Fe_{0.5}M_{0.5})SO_4F$ phases (M = Co, Ni, and Mn) only (see the Supporting Information for the complete series of the XRD). The related lattice parameters and cell volume data are summarized in Tables 4, 5, and 6, respectively, with the variation of the volume as a function of x shown in Figure 5. The substituting 3d-metals occupy the Fe-site in the FeO_4F_2 octahedra, keeping the 3-dimensional framework structure intact. On the basis of simple ionic radius considerations [Mn^{II} (97 pm) > Fe^{II} (92 pm) > Co^{II} (88.5 pm) > Ni^{II} (83 pm)][31] one would expect the unit cell volume to decrease with Co and Ni substitutions and to

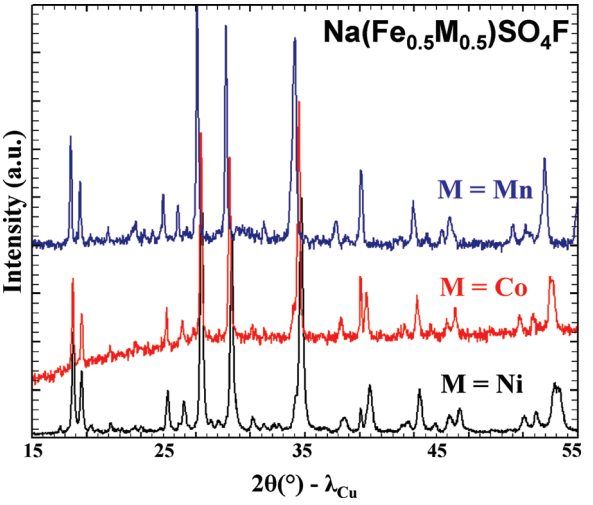

Figure 4. Comparative XRD patterns of 3d transition metal substituted sodium iron fluorosulphates for the $Na(Fe_{0.5}M_{0.5})SO_4F$ series for M = Co, M = Ni, and M = Mn. These compounds were prepared via solid state synthesis using equimolar mixtures of corresponding $(Fe_{1-x}M_x)SO_4 \cdot H_2O$ monohydrate precursors and NaF. The major impurity peak around 23° is due to the presence of $MSO_4 \cdot 4H_2O$ intermediate phases.

increase with the Mn substitution as we experimentally observed (Figure 5). Note also the existence of a complete solid solution for the Co- and Ni-based $Na(Fe_{1-x}M_x)SO_4F$ series having isostructural end members. In contrast, the solid solution does not extend beyond $x = 0.6$ for the $Na(Fe_{1-x}Mn_x)SO_4F$ series. This does not come as a surprise as $NaMnSO_4F$ is not isostructural with $NaFeSO_4F$. We could not extend the range of this solid solution regardless of whether we used solid-state or ionothermal synthesis routes. Besides, it is worth noting that we could not prepare these solid-solution phases either by ionothermal synthesis or by solid-state thermal treatment of a mixture of $NaFeSO_4F$ and

(30) Barpanda, P.; Chotard, J.-N.; Dupont, L.; Armand, M.; Tarascon, J.-M. *Chem. Mater.*, manuscript in preparation.
(31) http://www.webelements.com.

Table 4. Lattice Parameters and Cell Volume of $Na(Fe_{1-x}Co_x)SO_4F$ Solid Solution Phases Having Monoclinic ($P2_1/c$) Symmetry

materials	a (Å)	b (Å)	c (Å)	β (deg)	V (Å^3)
$NaFeSO_4F$	6.6799(2)	8.7060(2)	7.1914(2)	113.516(2)	383.48(2)
$Na(Fe_{0.8}Co_{0.2})SO_4F$	6.6759(4)	8.6804(3)	7.1742(3)	113.72(3)	380.62(4)
$Na(Fe_{0.6}Co_{0.4})SO_4F$	6.6721(9)	8.6632(2)	7.1612(5)	113.91(6)	378.39(4)
$Na(Fe_{0.5}Co_{0.5})SO_4F$	6.6760(6)	8.6634(5)	7.1564(3)	114.03(4)	378.02(3)
$Na(Fe_{0.4}Co_{0.6})SO_4F$	6.6698(5)	8.6534(4)	7.1535(3)	114.05(4)	377.02(2)
$Na(Fe_{0.2}Co_{0.8})SO_4F$	6.6670(7)	8.6392(3)	7.1458(3)	114.24(2)	375.27(6)
$NaCoSO_4F$	6.6664(3)	8.6174(4)	7.1436(3)	114.343(3)	373.89(3)

Table 5. Lattice Parameters and Cell Volume of $Na(Fe_{1-x}Ni_x)SO_4F$ Solid Solution Phases Having Monoclinic ($P2_1/c$) Symmetry

materials	a (Å)	b (Å)	c (Å)	β (deg)	V (Å^3)
$NaFeSO_4F$	6.6799(2)	8.7060(2)	7.1914(2)	113.516(2)	383.48(2)
$Na(Fe_{0.8}Ni_{0.2})SO_4F$	6.6632(5)	8.6616(6)	7.1671(2)	113.83(4)	378.37(3)
$Na(Fe_{0.6}Ni_{0.4})SO_4F$	6.6479(3)	8.6192(3)	7.1534(1)	114.04(1)	374.31(1)
$Na(Fe_{0.5}Ni_{0.5})SO_4F$	6.6397(2)	8.6024(1)	7.1391(4)	114.11(5)	372.17(5)
$Na(Fe_{0.4}Ni_{0.6})SO_4F$	6.6278(8)	8.5818(1)	7.1321(3)	114.18(2)	370.06(3)
$Na(Fe_{0.2}Ni_{0.8})SO_4F$	6.6193(9)	8.5503(2)	7.1078(6)	114.48(1)	366.11(6)
$NaNiSO_4F$	6.6099(3)	8.5252(3)	7.1032(1)	114.67(1)	363.72(1)

Table 6. Lattice Parameters and Cell Volume of $Na(Fe_{1-x}Mn_x)SO_4F$ Solid Solution Phases Having Monoclinic ($P2_1/c$) Symmetry

materials	a (Å)	b (Å)	c (Å)	β (deg)	V (Å^3)
$NaFeSO_4F$	6.6799(2)	8.7060(2)	7.1914(2)	113.516(2)	383.48(2)
$Na(Fe_{0.9}Mn_{0.1})SO_4F$	6.6970(9)	8.7156(2)	7.2088(7)	113.58(7)	385.62(9)
$Na(Fe_{0.8}Mn_{0.2})SO_4F$	6.7132(7)	8.7283(6)	7.2177(5)	113.71(3)	387.21(6)
$Na(Fe_{0.6}Mn_{0.4})SO_4F$	6.7298(8)	8.7360(7)	7.2475(7)	113.65(1)	390.30(7)
$Na(Fe_{0.5}Mn_{0.5})SO_4F$	6.7310(8)	8.7337(5)	7.2598(9)	113.76(5)	390.58(5)
$Na(Fe_{0.4}Mn_{0.6})SO_4F$	6.7437(6)	8.7464(6)	7.2787(4)	113.69(1)	393.15(5)
$Na(Fe_{0.2}Mn_{0.8})SO_4F$					
$NaMnSO_4F$	12.1635(5)	6.6364(2)	10.3488(4)	105.06(2)	806.65(5)

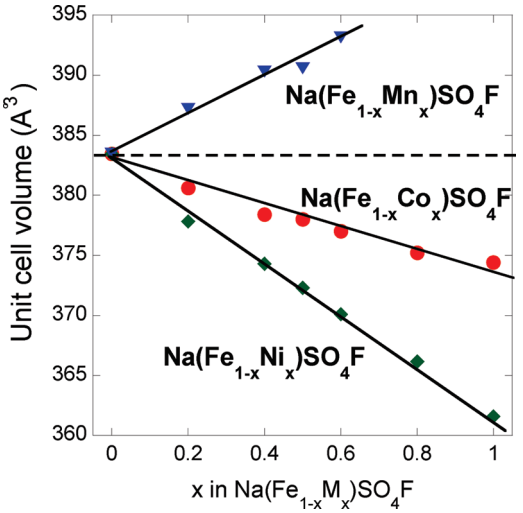

Figure 5. Graph showing the variation in the unit cell volume of 3d transition metal substituted $Na(Fe_{1-x}M_x)SO_4F$ (M = Co, Ni, Mn) compounds. Because of its larger size, Mn substitution increases the cell volume, whereas Co and Ni substitution results in decrease in unit cell volume. The black dashed line indicates the volume of pristine $NaFeSO_4F$ as a reference.

$NaMSO_4F$ end members, further signifying the importance of the underlying topochemical reaction (Supporting Information).

Synthesis of $(Na_{1-x}Li_x)MSO_4F$ Phases. The nature of alkali in these polyanionic metal fluorosulphate compounds ($AMSO_4F$, A = Na, Li) plays a pivotal role in shaping the orientation, symmetry, and final crystal structure because of its size and polarization. While Na favors a monoclinic structure ($NaMSO_4F$), the smaller and more polarizing Li tends to form a triclinic structure ($LiMSO_4F$) where the Li-ions are disordered over two sites occupied with equal probability. So a legitimate question regards the degree of compatibility between structurally different Li- and Na-based end phases, hence, the need to study the various $(Na_{1-x}Li_x)MSO_4F$ series with M = Fe, Co, and Mn.

As Mn-based fluorosulphates show identical monoclinic structures regardless of whether the guest alkali ion is Na or Li, we first attempted to prepare $(Na_{1-x}Li_x)MnSO_4F$ compounds via solid-state synthesis at 300 °C. The collected XRDs for the various members of the series are graphically presented in Figure 6a. There is a noticeable and gradual shift of the main Bragg peaks toward a lower angle, with increasing the Na content, implying the existence of a complete solid solution. However, a keen look reveals the possible presence of a narrow biphasic domain around $(Na_{0.5}Li_{0.5})MnSO_4F$. The shift toward the lower angle (e.g., higher d-spacing and larger unit cell volume, Figure 6b) is consistent with the fact of replacing small Li-ions (76 pm) by larger Na-ions (94 pm).[30] Thus, the increase in Na-content systematically leads to larger unit cell parameters as reported in Table 7.

Next, we attempted to synthesize the following $(Na_{1-x}Li_x)MSO_4F$ series (M = Fe and Co) bearing in mind that the Na- and Li-end members are not isostructural. The collected XRD profiles of Fe- and Co-based compounds were refined, and the corresponding lattice parameters reported in Table 8 and 9, respectively (only those for $x = 0.2$ and 0.3 are shown in Figure 7; refer to the Supporting Information for all compositions). Preparing mixed-cation Ni-based phases was relatively difficult. Whatever the nature of M, we were able to produce cationic solid-solution $(Na_{1-x}Li_x)MSO_4F$ phases

Table 7. Lattice Parameters and Cell Volume of $(Na_{1-x}Li_x)MnSO_4F$ Mixed Cation Solid Solution Phases Possessing Monoclinic ($I2/c$) Symmetry

materials	a (Å)	b (Å)	c (Å)	β (deg)	V (Å^3)
$NaMnSO_4F$	12.1635(5)	6.6364(2)	10.3488(4)	105.06(2)	806.65(5)
$(Na_{0.9}Li_{0.1})MnSO_4F$	12.2007(5)	6.6201(3)	10.3453(1)	105.35(8)	805.74(8)
$(Na_{0.8}Li_{0.2})MnSO_4F$	12.1549(5)	6.6327(7)	10.3373(3)	105.11(5)	804.54(0)
$(Na_{0.7}Li_{0.3})MnSO_4F$	12.1110(6)	6.5970(2)	10.2981(0)	105.29(4)	793.66(5)
$(Na_{0.6}Li_{0.4})MnSO_4F$	12.0789(8)	6.5600(3)	10.2749(3)	105.57(6)	784.27(2)
$(Na_{0.5}Li_{0.5})MnSO_4F$	12.0910(3)	6.5564(3)	10.2278(3)	105.49(8)	781.34(4)
$(Na_{0.4}Li_{0.6})MnSO_4F$	12.0256(0)	6.5174(5)	10.2028(8)	105.67(7)	769.94(5)
$(Na_{0.3}Li_{0.7})MnSO_4F$	11.9997(7)	6.4833(3)	10.1436(1)	105.72(6)	759.61(2)
$(Na_{0.2}Li_{0.8})MnSO_4F$	11.9605(9)	6.4651(5)	10.1519(7)	105.94(8)	754.80(5)
$(Na_{0.1}Li_{0.9})MnSO_4F$	11.9277(9)	6.4416(5)	10.1140(4)	106.06(7)	746.74(1)
$LiMnSO_4F$	11.8833(11)	6.4130(6)	10.0294(10)	106.15(3)	734.51(1)

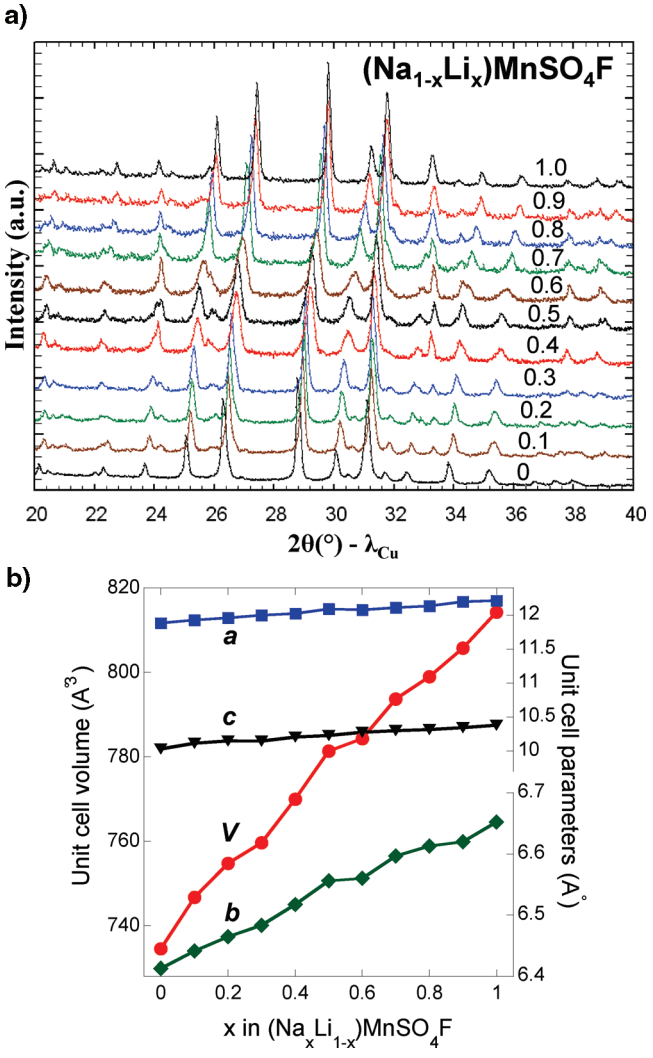

Figure 6. (a) Comparative XRD patterns of solid solution between $NaMnSO_4F$ and $LiMnSO_4F$, both having monoclinic structure with space group $P2_1/c$. The numbers alongside the patterns refer to the x value in $(Na_{1-x}Li_x)MnSO_4F$. (b) Graph showing the variation of cell parameters and cell volume of $(Na_{1-x}Li_x)MnSO_4F$ compounds as a function of Na content.

up to ~30% Li still bearing the monoclinic $NaMSO_4F$ structure in all cases with minor changes in lattice parameters. However, with higher Li content (40−100%), we systematically failed to form solid-solution phases despite several attempts both by solid-state and by ionothermal routes. Instead, a mixture of stoichiometric amount of $NaMSO_4F$ and $LiMSO_4F$ end phases was obtained. Interestingly, when we started from the Li-rich side and tried to substitute Li for Na, even a minute amount (say 5%) of Na-substitution led to the simultaneous (and independent) formation of Li- and Na- phases. From our experience, we observe that the triclinic $LiMSO_4F$-tavorite phases are on the verge of structural instability, and a slight distortion created by non-isostructural substitution results in structural decomposition or phase separation. A synergistic study of NMR and density functional theory (DFT) calculation may shed light on the structural instability of Li-rich $(Na_{1-x}Li_x)MSO_4F$ phases.

Thermal Analysis. Phosphate-based electrodes generally exhibit high thermal stability owing to the strong P−O and M−O bonds, which is crucial for safe battery operation. In our earlier report on $LiMSO_4F$ as well as $Li(Fe_{1-x}M_x)SO_4F$, we found that these compounds, as deduced by thermogravimetric and temperature-controlled XRD study, are stable up to 350 °C, amply sufficient for batteries but reflecting the lesser stability of the S−O bond.[10,18] Similar measurements were used to determine the thermal stability of $NaMSO_4F$ end members.

The TGA analysis (in air) of $NaMSO_4F$ end members is shown in Figure 8a. $NaFeSO_4F$ is stable up to 350 °C, after which there is a gradual weight loss, which can be due to the partial conversion of SO_4 species into SO_2 gas. The thermal degradation is more severe in case of $NaFeSO_4F$ (~16% weight loss) in comparison to $LiFeSO_4F$ (~5% weight loss), which indicates that the weaker bonding is associated with Na-based compounds. Other Na-homologues show similar nature, dissociating around 300 °C. $NaMnSO_4F$, which adopts a different XRD pattern than other homologues, have excellent thermal stability with little decomposition up to 600 °C in air (Figure 8a). As a rule of thumb, the reticular energy is usually higher for compounds having similar sized ions (cations and anions). Likewise for $NaMSO_4F$ phases, thermal stability should be higher for the compounds having the closest sized ions (i.e., M^{2+} cations and SO_4F^{3-} anions) knowing that Mn^{2+}, Fe^{2+}, and Co^{2+} have ionic radii of 97, 92, and 88.5 pm in octahedral coordination, respectively.[31] Besides, the observed stability for the Mn-based fluorosulphate can be further explained by the less reductive effect of Mn^{2+} as compared to the divalent Co and Fe ions. This reducing strength argument could also explain the observed stability of the Mg-based fluorosulphate at temperatures as high as 600 °C.

For further confirmation on thermal stability, a temperature-controlled XRD study was performed on a representative end member, that is, $NaFeSO_4F$ (as shown in Figure 8b). The pristine phase was retained up to 325 °C and decomposition started occurring ~350 °C, as depicted by the appearance of a few extra peaks. Further heating

Table 8. Lattice Parameters and Cell Volume of $(Na_{1-x}Li_x)FeSO_4F$ Mixed Cation Solid Solution Phases Possessing Monoclinic ($P2_1/c$) Symmetry

materials	*a* (Å)	*b* (Å)	*c* (Å)	α (deg)	*β* (deg)	*γ* (deg)	*V* (Å^3)
$NaFeSO_4F$	6.6799(2)	8.7060(2)	7.1914(2)	90.0	113.51(2)	90.0	383.48(2)
$(Na_{0.9}Li_{0.1})FeSO_4F$	6.6729(5)	8.7046(6)	7.1885(4)	90.0	113.48(8)	90.0	382.96(9)
$(Na_{0.8}Li_{0.2})FeSO_4F$	6.6717(6)	8.7005(9)	7.1893(6)	90.0	113.51(1)	90.0	382.66(4)
$(Na_{0.7}Li_{0.3})FeSO_4F$	6.6615(1)	8.6903(4)	7.1666(9)	90.0	113.64(7)	90.0	380.03(3)
$(Na_{0.6}Li_{0.4})FeSO_4F$							
$(Na_{0.5}Li_{0.5})FeSO_4F$							
$(Na_{0.4}Li_{0.6})FeSO_4F$							
$(Na_{0.2}Li_{0.8})FeSO_4F$							
$(Na_{0.1}Li_{0.9})FeSO_4F$							
$LiFeSO_4F$	5.1747(3)	5.4943(3)	7.2224(3)	90.0	107.2(3)	97.7(3)	182.55(1)

Table 9. Lattice Parameters and Cell Volume of $(Na_{1-x}Li_x)CoSO_4F$ Mixed Cation Solid Solution Phases Possessing Monoclinic ($P2_1/c$) Symmetry

materials	*a* (Å)	*b* (Å)	*c* (Å)	α (deg)	*β* (deg)	*γ* (deg)	*V* (Å^3)
$NaCoSO_4F$	6.6664(3)	8.6174(4)	7.1436(3)	90.0	114.343(3)	90.0	373.89(3)
$(Na_{0.9}Li_{0.1})CoSO_4F$	6.6824(5)	8.6423(6)	7.1469(3)	90.0	114.42(6)	90.0	375.81(6)
$(Na_{0.8}Li_{0.2})CoSO_4F$	6.6958(6)	8.6366(5)	7.1458(3)	90.0	114.49(5)	90.0	376.05(6)
$(Na_{0.7}Li_{0.3})CoSO_4F$	6.7019(7)	8.6337(7)	7.1482(3)	90.0	114.48(6)	90.0	376.40(6)
$(Na_{0.6}Li_{0.4})CoSO_4F$							
$(Na_{0.5}Li_{0.5})CoSO_4F$							
$(Na_{0.4}Li_{0.6})CoSO_4F$							
$(Na_{0.2}Li_{0.8})CoSO_4F$							
$(Na_{0.1}Li_{0.9})CoSO_4F$							
$LiCoSO_4F$	5.1721(7)	5.4219(7)	7.1842(8)	90.0	107.7(6)	97.9(5)	177.80(4)

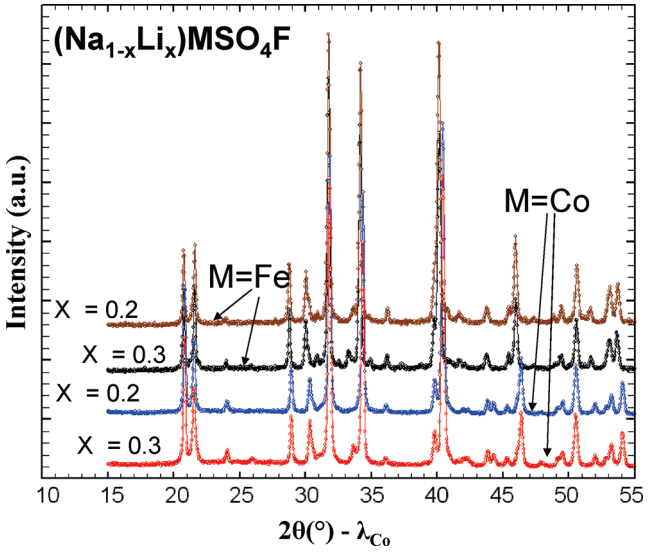

Figure 7. Comparative XRD patterns of solid solution between monoclinic sodium metal fluorosulphates and triclinic lithium metal fluorosulphates for the $x = 0.2$ and 0.3 members $(Na_{1-x}Li_x)MSO_4F$ series with M = Fe and Co. For M = Ni, it was difficult to produce $(Na_{1-x}Li_x)NiSO_4F$ phases, so they are not shown here.

aggravate the decomposition forming secondary phases like Fe_2O_3, Na_2SO_4, $Fe_2(SO_4)_3$, and FeS. From this study, a general conclusion can be drawn: all the $NaMSO_4F$ homologues as well as their derivatives are stable at least up to ≈325 °C.

Electrical Conductivity of $NaFeSO_4F$. Since the discovery of high ion mobility in sodium *β*-Al_2O_3 ($(Na_2O)_{1+x}\cdot 11Al_2O_3$),[32] there has been active search for superionic conductors for batteries and fuel cells. One such material system, colloquially termed as NASICON,[33−36] was introduced by Hong and Goodenough. As our materials have a Na-based polyanionic structure like NASICON although the 3D-packing is different, and knowing furthermore that conductivity is a key parameter for successful electrode application, we investigated the transport properties of $NaFeSO_4F$ $NaCoSO_4F$, and their solid-solution systems.

The conductivity results are summarized in Figure 9. Typical impedance spectra (Figure 9, inset) consist of a slightly depressed semicircle (at high frequency) and a defined Warburg diffusion tail (at lower frequency), suggesting the ionic nature of AC conductivity. This is further confirmed by the lower values of DC conductivity and the inability to measure DC conductivity at lower temperatures (300−340 K). The AC (ionic) conductivity value of $NaFeSO_4F$ was measured to be 7.14×10^{-7} S·cm^{-1} at ambient temperature (Figure 9a), which is four orders of magnitude higher with respect to $LiFeSO_4F$ (7.0×10^{-11} S·cm^{-1}).[10] The $NaFeSO_4F$ has a much lower AC activation energy (0.29 eV) in comparison to that of $LiFeSO_4F$ (0.99 eV). It is evident that these results on cold-pressed pellets suggest a bulk conductivity of several orders higher magnitude. NMR diffusion coefficient measurements are currently underway. The monoclinic structured $NaFeSO_4F$ has a rigid oxo-fluoride framework of corner-shared FeO_4F_2 octahedra and SO_4 tetrahedra. Such a high ionic transport suggests that the Na^+ ions are well connected by channels of low energy barriers allowing fast ion transport. Furthermore, unlike highly polarizing Li^+ that "sticks" to the walls of the galleries, Na^+, with a lower surface charge density, is likely to stay in the center as in *β*-alumina. This $NaMSO_4F$ structure permits a wide range of M-site substitution forming a versatile family of superionic conducting solids soon to be reported.[30] Ongoing first principle calculations

(32) Yao, Y. F.; Kummer, J. T. *J. Inorg. Nucl. Chem.* **1967**, *29*, 2453–2475.
(33) Tran Qui, D.; Capponi, J. J.; Gondrand, M.; Saïb, M.; Joubert, J. C.; Shannon, R. D. *Solid State Ionics* **1981**, *3*−*4*, 219–222.
(34) Hong, H. Y-P. *Mater. Res. Bull.* **1976**, *11*, 173–182.
(35) Goodenough, J. B.; Hong, H. Y-P.; Kafalas, J. A. *Mater. Res. Bull.* **1976**, *11*, 203–220.
(36) Padma Kumar, P.; Yashonath, S. *J. Chem. Sci.* **2006**, *118*(1), 135–154.

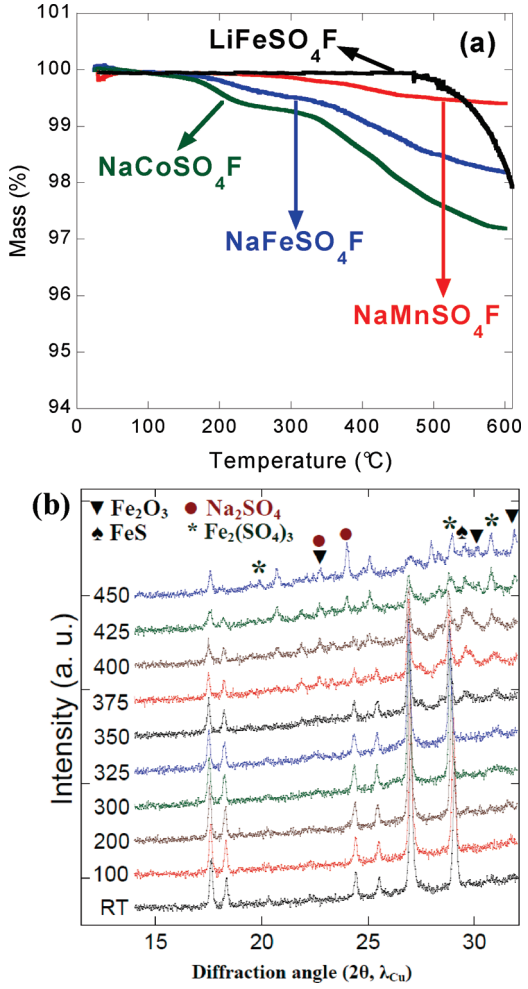

Figure 8. (a) Thermogravimetric analysis (TGA) of $NaMSO_4F$ homologues (M = Fe, Co, Mn) conducted from RT to 600 °C in air. Barring $NaMnSO_4F$, which is thermally stable, all other homologues decompose above 350 °C. The TGA curve of $LiFeSO_4F$ is also provided for reference. (b) Temperature-controlled XRD patterns of $NaFeSO_4F$ conducted from RT to 450 °C. The number along the XRD pattern refers to the heating temperature (°C). Several extra peaks start appearing after 350 °C (as marked) indicating thermal decomposition of parent material.

under the DFT + U framework should help in clarifying transport properties within this novel family of fluorosulphates.

Following, DC conductivity was tested by applying a steady external voltage of 1 V to the pellet and recording the steady-state current (i_{SS}), which is solely due to the electrons. Owing to low electronic conductivity, we could not measure any current below 80 °C, because of too small currents. Extrapolating the $\log(\delta) \sim (1000/T)$ curve, the DC conductivity value was measured to be 1.31×10^{-12} S cm^{-1} at ambient temperature, which is slightly lower than for $LiFeSO_4F$ (5.2×10^{-11} S·cm^{-1}). The DC activation energy for $NaFeSO_4F$ (0.70 eV) was comparable to that of $LiFeSO_4F$ (0.75 eV).

We observed similar values of AC and DC conductivity as well as activation energy values for $NaCoSO_4F$ (Figure 9c), further proving the superionic conductivity of these $NaMSO_4F$ phases. Eventually, we examined the transport properties of $Na(Fe_{1-x}Co_x)SO_4F$ solid-solution systems, using three intermediate compositions. As shown in Figure 9b, their AC (ionic) conductivity values are in the close proximity of 10^{-7} S cm^{-1}, with very similar values of activation energy. This affirms that these calcite-based $NaMSO_4F$ monoclinic phases have a very high ionic conductivity at room temperature. We are currently in the process of further investigating the transport properties of $NaMSO_4F$ phases, specially having a non paramagnetic metal center (M = Mg, Zn), using NMR spectroscopy.

Electrochemical Studies of Metal Fluorosulfates. To gauge the electrochemical activity and possibility of reversible Na^+ extraction from these novel fluorosulphate phases, we first conducted chemical oxidation of pristine $NaFeSO_4F$ with NO_2BF_4. Irrespective of the relative molar amount of NO_2BF_4, reacting time (1 to 4 days) or temperature (20−80 °C) at which the reaction was conducted, no chemical oxidation was observed, with the $NaFeSO_4F$ structure remaining intact (Supporting Information). This is somewhat surprising as very effective chemical oxidation has been earlier reported for Na-based compounds like Na_2FePO_4F, having a layered orthorhombic structure favoring facile Na extraction.[13] Besides, we also failed to perform any ion exchange by chemical reaction with excess LiCl or LiBr in ionic liquid/acetonitrile/cyclopentadione medium (Supporting Information). For both $NaFeSO_4F$ and $NaCoSO_4F$, there was absolutely no success in Na-ion exchange by Li.

Next, the $NaFeSO_4F$ end member was tested in an electrochemical cell to check its activity. An 80:20 powder mixture of $NaFeSO_4F$ and SP carbon black was cycled at C/20 rate in a sodium cell. Though $NaFeSO_4F$ has a theoretical capacity of 137 mAh·g^{-1}, we could hardly achieve ~6% of capacity (Figure 10a). Like $LiFeSO_4F$, $NaFeSO_4F$ too has a Fe^{II}/Fe^{III} signature plateau centered around 3.6 V. The other $NaMSO_4F$ (M = Co, Ni, Mn) homologues were cycled up to 5 V in Swageloks, still giving no redox reaction. A point to note is that we used solid-state synthesized $NaFeSO_4F$ for electrochemical study, which gives similar results to the ionothermal synthesized $NaFeSO_4F$, as there is no particle coarsening/grain-growth at moderate temperature of 300 °C.

As $LiFeSO_4F$ delivers excellent electrochemical cycling,[10] we prepared chemically oxidized $Li_{0.75}FeSO_4F$, $Li_{0.25}FeSO_4F$, and $FeSO_4F$ from parent $LiFeSO_4F$. These materials were cycled in a sodium cell architecture with 1 M Na-TFSI:PC electrolyte to notice the effective Na insertion capability. The resulting electrochemical curves are shown in Figure 10b (and Supporting Information). Similar to earlier data, we observe very inefficient Na-insertion into these materials upon cycling. Overall, at this nascent stage, sodium metal fluorosulphates are electrochemically limited, the main reason being most likely associated to their structures as discussed next.

Discussion

We have exploited the rich chemistry offered by the fluorosulphate to successfully prepare novel Na-based 3d metal fluorosulphates $NaMSO_4F$ (M = Fe, Ni, Mn, and Co). Such phases structurally differ from their Li counterparts previously reported as they crystallize in a monoclinic ($P2_1/c$) rather than in a triclinic ($P\bar{1}$) structure except for Mn which crystallizes in a monoclinic cell whose space group has not yet been determined. Such a Na-driven triclinic-monoclinic transition, which is associated with a unit cell volume of ≈9 Å^3 from $LiFeSO_4F$

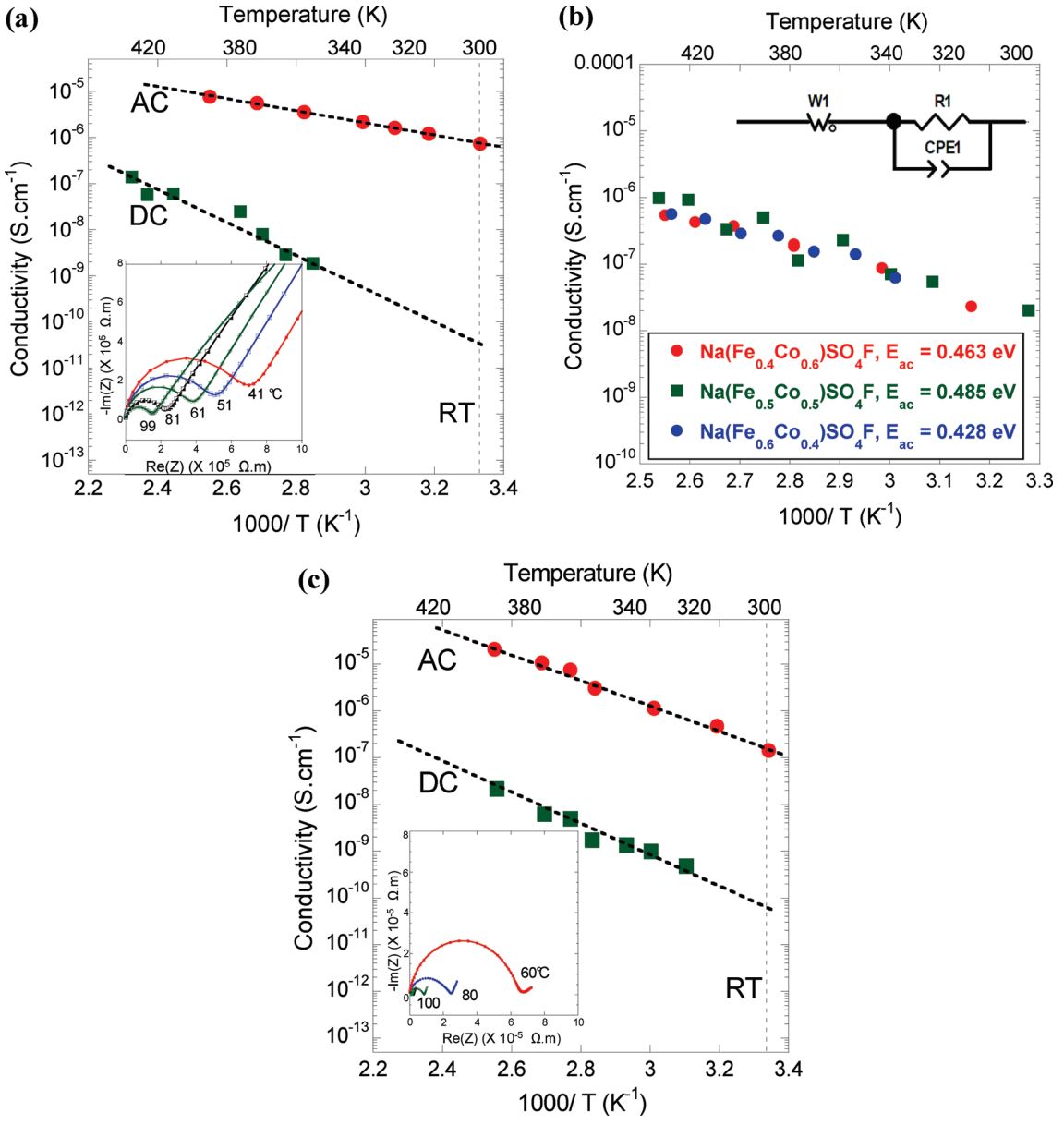

Figure 9. (a) Conductivity of $NaFeSO_4F$ pellet at different temperatures coated with ionically blocking Au electrodes. Inset image shows representative AC impedance spectra (Nyquist plot). They have a slightly depressed high-frequency semicircle and a low-frequency Warburg diffusion line. (b) The AC conductivity values of three compositions in $Na(Fe_{1-x}Co_x)SO_4F$ (x = 0.4, 0.5, 0.6) solid-solution system with their AC activation energy reported. The inset image at top right corner shows the equivalent circuit consisting of a resistance (R1) and a constant phase element (CPE1) in parallel connection, along with Warburg resistance (W1). The ionic conductivity value was calculated from the resistance of high-frequency semicircle. (c) Conductivity of ionically blocking $NaCoSO_4F$ pellet at different temperature having similar transport properties as $NaFeSO_4F$.

(182.56 Å^3) to $NaFeSO_4F$ (191.73 Å^3), is most likely nested in the larger ionic radii of Na^+ as compared to Li^+.

Although all of these structures preserve the same sequence of octahedral (FeO_4F_2) and tetrahedral (SO_4) arrangements, they differ by subtle reorientations of these polyhedra with respect to each other as well as by the position of the alkali atom which is disordered over two different sites occupied at 50% for Li as compared to a single site for Na. From studies of the alkali [$(Na_{1-x}Li_x)MSO_4F$] and 3d-metal [$Na(Fe_{1-x}M_x)SO_4F$] substituted series, we show the inability to substitute any Li for Na in the end member $LiMSO_4F$ (M = Fe, Co, Ni) phase showing its resilience against sodium substitution while solely 0.3 Na can be replaced by 0.3 Li in the end solution member $NaMSO_4F$ phases. As most of these phases are not stable for temperatures greater than ≈325 °C, we could at first attribute such failure to our solid-state synthesis process, but it is not so since no noticeable differences were found with respect to the extent of the obtained solid solution when the samples were made by ionothermal synthesis. Such a limited solubility existence for the end-member phases prepared at 300 °C is reflective of what does occur at room temperature as well, since we could not succeed in electrochemically removing at room temperature more than 0.2 Na from $NaFeSO_4F$ and replacing it by the equivalent amount of Li. More so, the limited tolerance of the triclinic ($P\bar{1}$) structure to sodium is reflected by our inability to reversibly insert more than 0.2 Na ions in our fully delithiated $FeSO_4F$ structure.

In contrast, our ability to prepare the full $(Na_{1-x}Li_x)MnSO_4F$ solid solution is not a surprise as both end members ($LiMnSO_4F$ and $NaMnSO_4F$) have a monoclinic structure;

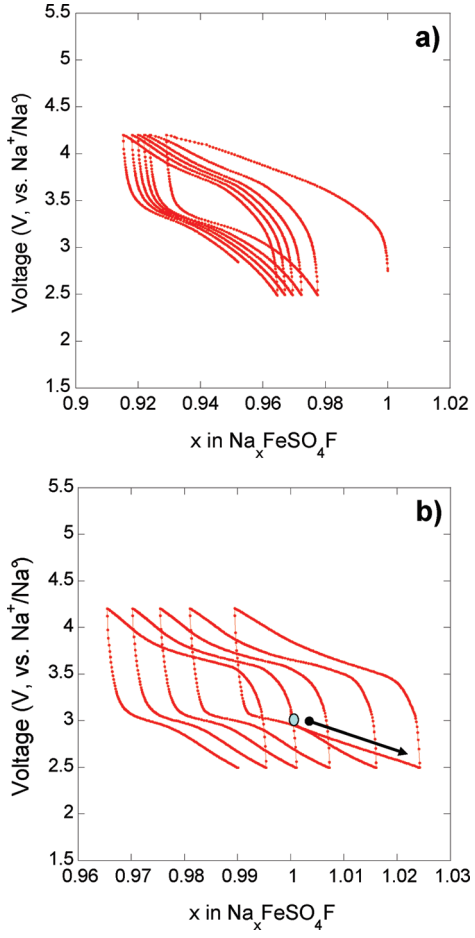

Figure 10. (a) Electrochemical voltage profile of $NaFeSO_4F$ cycled in a sodium cell with metallic Na anode and 1 M Na-TFSI:PC electrolyte at a rate of $C/20$. The $NaFeSO_4F$ was prepared by the solid-state route, and the electrode was made by ball-milling $NaFeSO_4F$ and SP carbon black on 80:20 ratio for 10 min. (b) Electrochemical voltage profile of chemically delithiated $LiFeSO_4F$ powders cycled in a sodium cell with metallic Na anode and 1 M Na-TFSI: PC electrolyte at a rate of C/20.

neither is the existence of a complete solid solution among the 3d-metal [$Na(Fe_{1-x}M_x)SO_4F$] substituted series, as the end members $NaFeSO_4F$ and $NaMSO_4F$ (M = Co, and Ni) adopt the same monoclinic structure. We presently view our 60% limited Mn solubility in $Na(Fe_{1-x}Mn_x)SO_4F$ series as a strong indication of a different space group for the two end members monoclinic unit cells. Synchrotron experiments are presently being planned to clarify this point.

Turning to the transport properties, we found $NaFeSO_4F$ to show a drastically higher ionic conductivity ($\approx 7.14 \times 10^{-7}$ $S \cdot cm^{-1}$) than its Li counterpart ($\approx 7 \times 10^{-11}$ $S \cdot cm^{-1}$ for $LiFeSO_4F$). This comes as a surprise from structural considerations as (i) the sodium ions are less disordered than the lithium ones in the structure and (ii) the 3D-channels displayed by the $NaFeSO_4F$ phase for sodium migration are less open than those displayed by the $LiFeSO_4F$, namely, along the [111] direction; both of these observations lead to the expectation of a lower ionic conductivity for the Na phase. This is an expectation initially supported by our inability to exchange sodium for Li into the Na-based phase or even to remove Na from these compounds regardless of the oxidant we have tried. Thus, such a counter intuitive greater ionic conductivity measured for the Na-phase as compared to the Li-one is worth of further consideration. The fact that Na^+ could be more mobile than Li^+ could be nested, like for beta-alumina, in a better fit of Na^+ cations to the size of the galleries. We must on the other hand make certain that the other singly charged ion, F^-, is not the charge carrier. Fluoride is appreciably mobile in fluorite-type compounds, especially with soft Pb^{2+} or Sn^{2+}, but the more polarizing transition metals are unlikely candidates, independently of the favorable tunnel structure. NMR experiments are underway with the Zn or Mg equivalents, as the paramagnetic d-cation screen the signal and will be reported within the scope of a systematic investigation of ionic conductivity in theses new host structures.

Prior to carrying on the above track, it should first be recalled that ion size consideration does not universally rule ionic conductivity, with the best example against it being the highest conductivity in Na-β alumina than either Li or K counterparts. Besides, high ionic conductivity and limited insertion properties are not incompatible within a poorly electronic conducting electrode material, as redox reactions require both electronic and ionic conducting properties. Regarding insertion reactions, they can enlist either solid solutions or two-phase reactions depending upon whether the fully lithiated or delithiated phases have the same structure. Interestingly, the monoclinic $NaFeSO_4F$ phase has a volume of 191.73 $Å^3$ as compared to 163.64 $Å^3$ for the triclinic ($P\bar{1}$) delithiated phase. Therefore, the removal of sodium implies a huge volume contraction ($\approx$16%) associated to a phase change, which is energetically unfeasible, and this is the reason why such a Na deintercalation process does not proceed. To this end, existing computer modeling methods, such as quantum chemical calculations using DFT procedures, are intensively needed to provide a rationale for the stability of these phases and for their redox reactions and transport features. Undoubtedly, the richness and complexity of the structural behavior of these fluorosulphates will challenge DFT promoters.

Conclusions

The synthesis of various sodium metal fluorosulphate compounds is reported for the first time. Using both low temperature solid-state synthesis and ionothermal synthesis, different end members ($NaMSO_4F$, M = Fe, Co, Ni, Mn) were prepared at a moderate temperature of 300 °C, and their monoclinic structures were solved. Owing to the isostructural nature, various 3d transition metals (Co, Ni and Mn) could be substituted to the Fe site to form series of $Na(Fe_{1-x}M_x)SO_4F$ (M = Co, Ni, Mn) phases. All these sodium-based phases were found to be monoclinic, unlike their lithium counterparts. These phases were found to be structurally sensitive; thus, we were unable to formulate a complete series of solid-solution $(Na_{1-x}Li_x)MSO_4F$ phases. With open tunnel structures, the $NaFeSO_4F$ compounds were found to have excellent ionic conductivity ($\sim 7.14 \times 10^{-7}$ $S \cdot cm^{-1}$), which is impressive for solid-state electrochemical applications. However, we could extract only 0.7 Na from this structure electrochemically involving a 3.6 V Fe^{II}/Fe^{III} redox plateau. We hope that this paper, which highlights the richness of the fluorosulphate crystal chemistry together with their attractive ion transport properties, will call for intense theoretical calculations using DFT procedures or others so as to boost our research for better ionic conductors.

Acknowledgment. The authors would like to thank M. Courty, M. Reynaud, K. Djellab, W. Walker, C. Masquelier, E. Baudrin, and J.-B. Leriche for their technical assistance and the ALISTORE-ERI nanopositive team members for fruitful discussions. J-M.T. is grateful to F. Wudl's group for hosting him and sharing their laboratory synthesis facilities as well as Materials Research Laboratory (MRL) for use of their XRD equipment at the University of California Santa Barbara (UCSB). The authors further acknowledge Ms. Michèle Nelson for proof-reading and improving the linguistic aspects of the article.

Supporting Information Available: Further details are given in Figures S1−S8 and Table S1. This material is available free of charge via the Internet at http://pubs.acs.org.